PAPER

High temperature, transparent, superhydrophobic Teflon AF-2400/Indium tin oxide nanocomposite thin films

IOP Publishing Nanotechnology
Nanotechnology 30 (2019) 175702 (14pp) https://doi.org/10.1088/1361-6528/aaf262

High temperature, transparent, superhydrophobic Teflon AF-2400/Indium tin oxide nanocomposite thin films

Raad A Alawajji, Ganesh K Kannarpady[1], Zeid A Nima, Nigel Kelly, Fumiya Watanabe and Alexandru S Biris[1]

Center for Integrative Nanotechnology Sciences, University of Arkansas at Little Rock 2801 South University Avenue, Little Rock, AR 72204, United States of America

E-mail: gkkannarpady@ualr.edu and asbiris@ualr.edu

Received 10 August 2018, revised 9 November 2018
Accepted for publication 20 November 2018
Published 15 February 2019

Abstract

The outstanding properties of Teflon AF-2400—chemical, optical, etc—inspired us to make modifications to enhance its hydrophobicity. We prepared an AF-2400/indium tin oxide (ITO) nanocomposite by a spin coating technique at room temperature, using the AF-2400 polymer as the matrix and ITO nanoparticles as the filler. Different ITON concentrations ranging from 3 to 30 mg ml^{-1} were prepared to study the effect of nanoparticle loading on the films' properties and superhydrophobicity. The effect of spin speed and annealing temperature was also studied. Atomic force microscopy, x-ray photoelectron spectroscopy, and UV–vis analysis were employed to characterize the prepared films. The results indicated that the film's low surface energy and nano/micro-features made it superhydrophobic. Increasing the ITON concentration to 15 mg ml^{-1} improved the superhydrophobicity of the composite film by increasing the surface roughness. The coating showed superhydrophobic behavior with a static contact angle (SCA) around 152° and contact angle hysteresis less than 2°. The nanocomposite films also exhibited excellent thermal stability, sustaining temperatures as high as 240 °C without losing their superhydrophobic behavior. Three models, Wenzel, Cassie–Baxter, and Shuttleworth–Bailey, were used to predict the SCA. The results confirmed that the latter model gave the best prediction. In addition to superhydrophobicity, the AF-2400/ITON films coated on a glass substrate showed very high transparency—around 95% in the visible and infrared ranges. An effective medium theory, the Bergman representation, was used to simulate the transmittance of the AF-2400/ITON nanocomposites. The measured and simulated transmittance values were in good agreement in the visible range. Based on our results, this coating may be highly useful for many practical applications, including solar cell coatings, chemical resistance protective coatings, and more.

Keywords: optically transparent coating, Teflon AF, high temperature superhydrophobic coating, indium tin oxide, nanocomposite

(Some figures may appear in colour only in the online journal)

1. Introduction

The need for transparent, superhydrophobic coatings is growing in a wide range of applications, such as consumer electronics, automobile windshields, camera lenses, and high-resolution displays and monitors. Surfaces that exhibit contact angles over 150° and contact angle hysteresis (CAH) less than 10° are typically superhydrophobic, meaning that water droplets bounce off them. Additionally, fabrication of superhydrophobic surfaces that are also transparent and protect

[1] Authors to whom any correspondence should be addressed.

against chemical corrosion and other environmental effects is both highly needed and highly challenging. Integrating such surfaces onto an active application area is a complex process requiring the coating materials to be rugged and resistant to environmental organics and pollutants. Several attempts have been made by researchers to develop transparent, superhydrophobic coatings. Xu *et al* synthesized transparent, superhydrophobic coatings by spin coating fluorosilane-modified silica nanoparticles [1]. They showed that their spin-coated nanoparticles produced a better superhydrophobic surface than dip-coated nanoparticles. However, as noted in their paper, the surface suffered from lack of adhesion. In another study, Ebert and Bhushan fabricated wear-resistant, superhydrophobic, transparent coatings on glass and polymer substrates using SiO_2, ZnO, and ITO nanoparticles. While these coatings showed excellent superhydrophobic properties, their transmission behavior in the visible range deviated largely from that of the substrates [2].

Bharathibai and Kumer incorporated modified silica particles in a polytetrafluoroethylene (PTFE) emulsion in order to generate superhydrophicity. They showed that the silica particle concentration controlled the superhydrophobicity, with the contact angle reaching ∼165° and the low sliding angle less than 2° [3]. In a different study, sandpaper was used to promote the superhydrophobicity of a PTFE sheet [4]. The technique was easy, inexpensive, and able to create a surface with a water contact angle of up to 151° and sliding angle less than 4°. Varying the grit size of the sandpaper affected the surface's contact angle and hysteresis. Kewie *et al* developed a nanocomposite base on a carbon nanotube and PTFE resin by spray coating. The film showed enhanced wear resistance with a contact angle of 154.1° and CAH less than 2° [5]. Zhuang *et al* used aerosol-assisted chemical vapor deposition to generate superhydrophobic PTFE films, with the contact angle reaching 168° and optical transmission reaching over 92%. These films were wear-resistant, capable of withstanding rigorous water droplet impingement and sand grains [6]. Finally, our own group recently used pulsed laser deposition (PLD) to fabricate a transparent PTFE superhydrophobic coating on glass substrates [7]. The roughness obtained by laser ablation combined with the low surface energy of PTFE resulted in a high contact angle of around 150° and CAH of about 2°. The films showed optical transmission over 90% in the visible region. However, scaling up PLD/chemical vapor deposition is expensive, and this technique could only be used for specialized applications.

Teflon® AF is a unique family of amorphous fluoroplastics based on a copolymer of TFE (tetrafluoroethylene) and PDD (2,2 bistrifluorommethyl-4,5 difluoro-1,3 dioxole), having the chemical structure shown in figure 1. This family of amorphous polymers shares many of the extraordinary properties of fluoro-polymers, such as high temperature stability, low surface energy and water absorption, and outstanding chemical resistance. The main difference between traditional fluoroplastics such as PTFE, PFA, and FEP and Teflon® AF is the degree of crystallinity. The semi-crystalline or highly crystalline fluoroplastics (PTFE, PFA, etc.) are

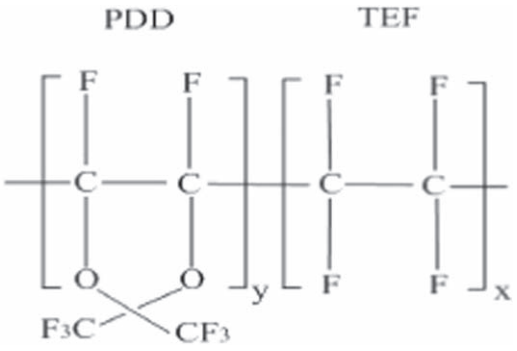

Figure 1. Chemical structure of Teflon®AF.

soluble only in high-boiling per-fluorocarbon solvents at a temperature near their melting point [8]. Therefore, only certain techniques can be used to create thin films from these kinds of fluorocarbon polymers, such as sputtering [9], PLD [10], and chemical vapor deposition [11]. Unlike PTFE, Teflon®AF is an amorphous polymer that is soluble in various per-fluorinated solvents at room temperature. This enhanced polymer solubility results from the incorporation of an oxygen group in the polymer's chemical structure. Because of its solubility, Teflon® AF can be used to make very thin and homogenous coatings via various methods, including spin coating, dip coating, and spray coating [8, 12]. Also, these polymers are considered the most transparent materials, with high transmission over a broad range of wavelengths.

Commercially, two different types of Teflon™ AF polymers are available, AF-2400 and AF-1600. The dioxole monomer content (87% for AF-2400 and 65% for AF-1600) determines the physical properties of these polymers. For instance, depending on the PDD content, the transition temperature for AF-2400 is ∼240 °C and ∼160 °C for AF-1600. Additionally, the optical properties of these polymers can be controlled systematically by adjusting the TEF/PDD percentage [13]. Teflon® AF thin layers have been used as anti-reflective coatings for potassium di-hydrogen phosphate (KDP) crystals and other optical materials because they have a very low refractive index (∼1.29) and excellent transmission properties in a wide range (200–2000 nm) [12, 14]. Furthermore, the low refractive index of Teflon™ AF-2400 compared with the refractive index of water ($n_D = 1.33$) makes it an incredibly useful cladding layer to provide better performance in liquid waveguide applications [15–17].

Teflon® AF polymers are showing greater promise for many practical applications than other organic polymers because of their extremely low water uptake and surface energy. Teflon® AF polymers exhibit low water absorption (<0.01%), making them unaffected by moisture. Additionally, AF-2400 has the lowest surface free energy of all homogenous polymers [18]. These traits have led researchers to use the polymers to make superhydrophobic materials. It was reported that varying the thickness of a Teflon® AF-1600 film from 17 to 420 nm by increasing the number of layers using spin coating had essentially no effect on the film's contact angle [19]. Other research has shown that controlling the topography and spontaneous wrinkling of Teflon® AF by

a thermal annealing process produced a superhydrophobic film with a contact angle of around 170° and CAH less than 2° [20]. In another study, carbon nanotubes were dispersed in Teflon® AF to produce a superhydrophobic solution used to coat fabrics. The static contact angle (SCA) of the coated fabric was greater than 150°, and the receding angle was less than 15° [21].

Here, we present a novel technique for fabricating Teflon® AF-2400-ITON nanocomposite films that exhibit high optical transmission, superhydrophobicity, and SCAs over 152°, with water bouncing off the surface. ITO was chosen as the filler material due to its proven viability in commercial applications, as well as excellent optical transparency, electrical conductivity, and thermal stability. The nanocomposite is rugged and capable of withstanding temperatures as high as 250 °C without losing its superhydrophobicity. The nanocomposite films are transparent in a wide range of wavelengths. The optical properties of the films were mathematically modeled using W. Theiss hard- and software. The surfaces' wetting properties were modeled using Wenzel, Cassie–Baxter, and Shuttleworth–Bailey models.

2. Experimental Methods

2.1. Materials

Amorphous fluor-polymer AF-2400 in powder form was purchased from DuPont Co. USA. Fluorinert FC-40 solvent (density 1.85 g cm^{-3}, B.P. 155 °C) was procured from 3 M Company. Indium tin oxide (ITO) nano powder, In_2O_3 90%, SnO_2 10%, and particle size <50 nm, was purchased from Sigma Aldrich. Microscope glass slides were purchased from Fisher Scientific. Millipore membrane paper and hydrophilic mixed cellulose filter paper (5 μm pore size, 5 cm diameter) were purchased from Sigma Aldrich.

2.2. Sample preparation

First, glass substrates were cut to proper size (25 mm × 25 mm), cleaned with acetone and ethanol, rinsed with deionized (DI) water to remove organic residues, and dried with compressed nitrogen. After that, the following three steps were completed to prepare the AF-2400/ITON nanocomposite.

In the first step, 1.5% solution by weight of Teflon® AF-2400 in fluorinert FC-40 solvent was prepared by stirring Teflon® AF-2400 powder in the solvent at 50 °C. Due to the high molecular weight of Teflon® AF-2400, the solution was stirred for 48 h to ensure complete dissolution. Then, the prepared solution was filtered using the membrane (pore size 5 μm) to remove undissolved or aggregated particles. In the second step, the ITONs were mixed with the Teflon® AF-2400 solution at different ITON concentrations (0–30 mg ml^{-1}). The AF-2400/ITON mixture was stirred for 1 h at 2000 rpm at room temperature. In order to obtain a uniform dispersion of ITONs, the mixture was then sonicated for 30 min. In the final step of preparation, 100 μl of the AF-2400/ITON mixture was spun at 1000 rpm for 30 s onto glass substrates using a spin coater (Model Ws-400E-6Npp-LITE). The spinning speeds were varied between 1000 and 6000 rpm for 30 s to obtain different film thicknesses. Then, the coated glass substrates were left to dry in air for 15 min, followed by baking on a hotplate at 100 °C for 30 min to remove the solvent from the samples. In order to study the effect of annealing temperature on optical and wetting properties, the nanocomposite films with ITON concentration of 15 mg ml^{-1} were annealed on a digital hotplate for 60 min at various temperatures in the range of 100 °C–330 °C.

2.3. Measurements and characterizations

The SCA and CAH of the samples were measured using an EasyDrop (DSA1) device (Kruss Co.) by the sessile drop method. The CAH was estimated by measuring the advancing and receding contact angles using the relation CAH = advancing angle − receding angle. For every sample, 5-μl DI water droplets were dispensed gently via computer-controlled syringe at four different places on the glass substrates. A CCD camera was used to capture images of the water droplets. The contact angles at the four spots were averaged and presented with the standard deviation. All the contact angles were measured at room temperature.

The surface chemical composition of the AF-2400/ITON films was characterized by x-ray photoelectron spectroscopy (XPS) (Thermo Scientific K-Alpha), equipped with an Al Kα x-ray source (1430 eV). The pressure in the chamber was lowered to 1×10^{-11} Torr during data collection. The data were collected from a 20 μm × 20 μm area on the samples in order to detect the surface elemental percentage of the prepared films in the range of 0–1200 eV.

The surface morphology and the film thickness of the prepared samples were analyzed by atomic force microscopy (AFM, Bruker Dimension Icon FastScan). The data were collected by scanning the surface with a silicon tip connected to a soft cantilever (resonance freq.: 300 KHz, force constant: 40 N m^{-1}) moving in x, y, and z directions. Tapping mode was used, with a scan rate of 1 Hz and scan area of 1 μm × 1 μm. The images were analyzed by Nano-Scope Analysis software (ver.1.5). Similarly, scanning electron microscopy (SEM, JEOL JSM-7000 F) and energy dispersive spectroscopy (EDS) were used to study the surface morphology and elemental mapping of the films.

Transmittance measurements for the AF-2400/ITON-coated glass substrates were taken using UV–vis-NIR spectroscopy (Shimatzu-3600) at wavelengths ranging from 300–1000 nm. Scout software (from W. Theiss hard- and software) was utilized to simulate the optical transmission behavior of the samples.

3. Results and discussion

3.1. Wetting behavior

The wetting behavior of the AF-2400/ITON-coated glass substrates was analyzed based on the contact angle

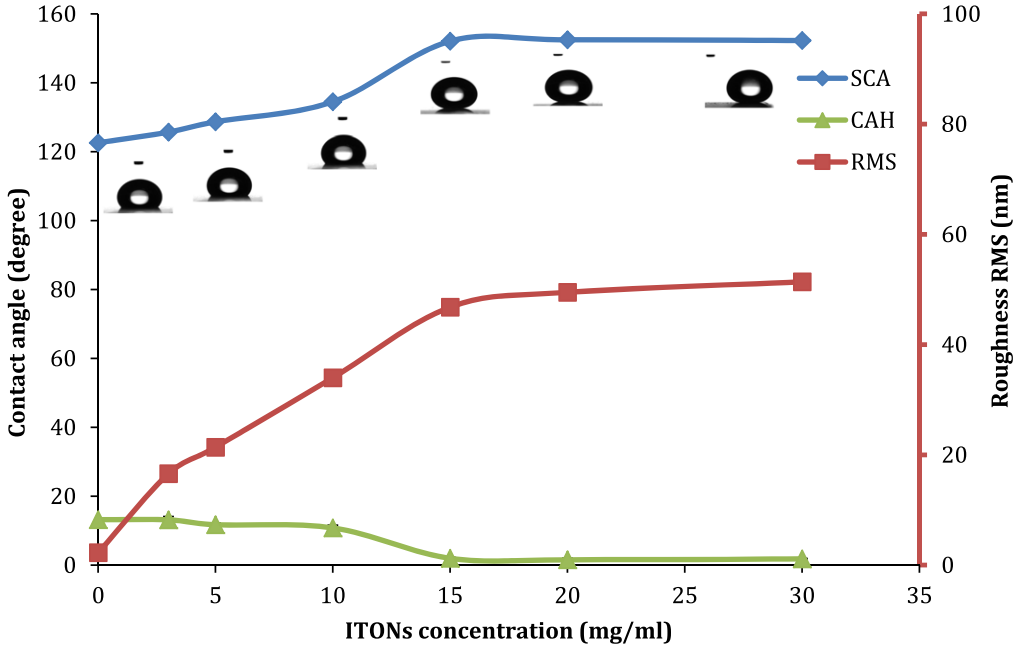

Figure 2. Static contact angle, contact angle hysteresis, and surface roughness of pure AF-2400 and AF-2400/ITON thin film-coated glass substrates as a function of ITON concentration. Insets are the water droplets (5 μl) on the films' surface.

measurements of water droplets deposited on their surfaces. Figure 2 presents the SCA, CAH, and roughness (RMS) of the pure AF-2400 and AF-2400/ITON thin films as a function of ITON concentration. The SCA of the AF-2400 film was 122° ± 0.5° and the CAH around 13° ± 1°. When a small amount of ITON (below 10 mg ml^{-1}) was added, the SCA increased steadily and the CAH decreased. This behavior (low SCA and high CAH) for the pure AF-2400 films and the films with low ITON loading is caused by the very smooth surface of the films, which had roughness around 2.26 nm (figure 2). As the ITON concentration reached 10 mg ml^{-1}, the SCA increased to 134° ± 0.5° with CAH around 10° ± 0.5°. A steady increase in surface roughness was observed. When the ITON concentration increased to 15 mg ml^{-1}, the film began showing superhydrophobicity, with a SCA of ∼152° ± 0.1° and CAH around 1.7° ± 0.2°. This behavior is attributed to the increasing surface roughness; high ITON loading caused air pockets to form on the surface. These air pockets trapped air on the film surface, helping to lower the surface energy of the AF-2400/ITON thin film and promote superhydrophobicity. An ITON concentration above 15 mg ml^{-1} resulted in the SCA and CAH plateauing. A similar trend was observed for the surface roughness (figure 2).

In order to show the effect of film thickness on SCA, we studied the nanocomposite films (15 mg ml^{-1}) as a function of spinning speed. We chose this concentration because the SCA plateaued at it, as shown in figure 2. Figure 3 illustrates that increasing the spinning speed gradually decreased the thickness of the AF-2400/ITON nanocomposite films, as expected. Figure 3 also gives the variation in contact angle as a function of spinning speed. The SCA followed a similar trend as the film thickness, decreasing as spinning speed increased. The contact angle remained almost plateaued when the spinning speed was below 4000 rpm, then started decreasing dramatically as the spinning speed increased above 4000 rpm. This may be due to reduction in the film thickness at high spinning speed, which caused islands of AF-2400 matrix and ITONs. As a result, water droplets would partially sit directly on ITONs that were not well covered by AF-2400, reducing the contact angle drastically. According to these results, we concluded that a spinning speed of 3000 rpm produces the highest SCA.

Additionally, we studied the ability of the AF-2400/ITON composite films to withstand high temperatures. This factor is important because temperature enhances the adhesion and other properties of AF-2400. There are several applications, such as automobile windshields, in which transparent, superhydrophobic coatings that can be frequently exposed to high temperatures are desirable. Figure 4 displays the effect of annealing temperature on the superhydrophobicity of the composite films. The SCA remained stable around 152° when the annealing temperature was below 250 °C. Raising the temperature above 240 °C caused changes in film morphology and roughness, leading to a drop in contact angle to 138° ± 1° at 330 °C.

3.2. Surface morphology and elemental mapping

AFM was used to study the effect of surface morphology on the superhydrophobicity of the composite films. Figure 5 shows 3D images of pure AF-2400 and AF-2400/ITON nanocomposite films with different ITON concentrations. The pure AF-2400 film was relatively smooth and homogenous, with roughness (RMS) around 2.26 nm. The film was just hydrophobic, a trait that can be attributed to its chemical

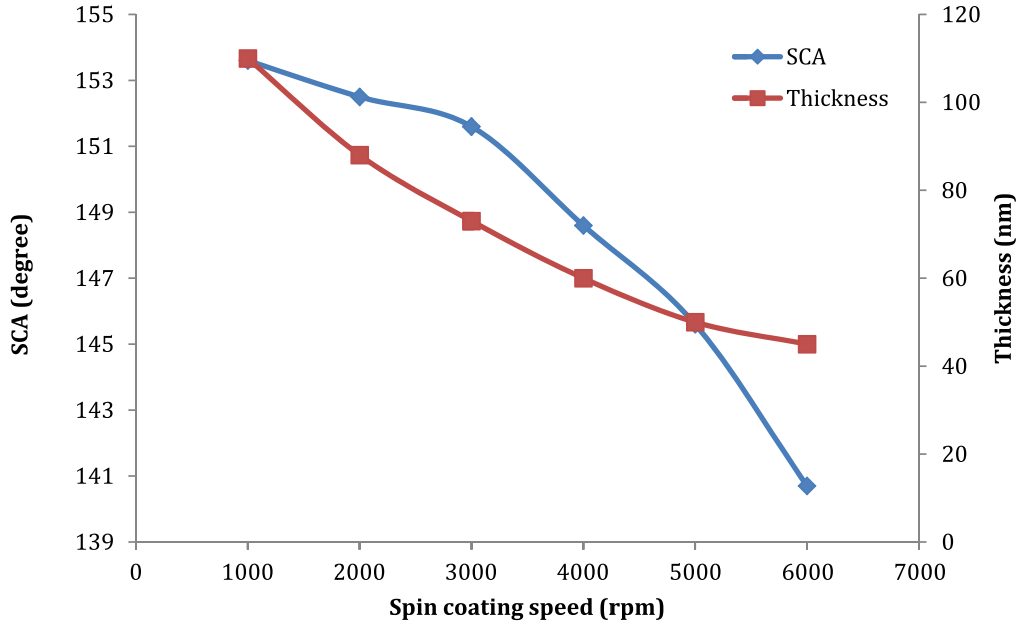

Figure 3. Static contact angles of AF-2400/ITON thin films and the thickness of a 15 mg ml^{-1} sample as a function of spin coating speed. Contact angles were measured at 10 different places for each film, and the standard deviation was ±1.5°.

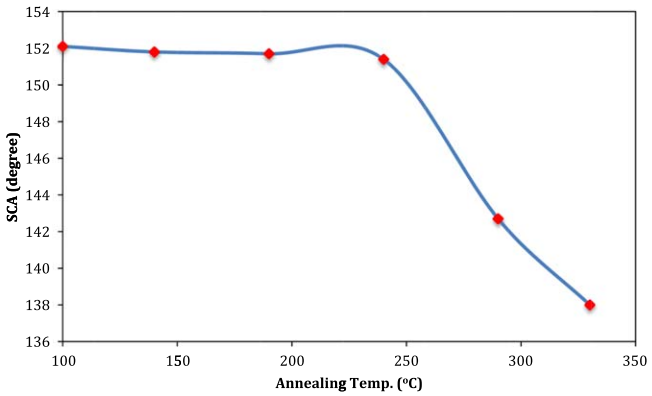

Figure 4. Effect of annealing temperature on static contact angles of AF-2400/ITON nanocomposites with 15 mg ml^{-1} ITON concentration. Contact angles were measured at 10 different places for each film, and the standard deviation was ±1.5°.

nature. The film's surface roughness gradually increased as the concentration of ITONs in AF-2400 increased. As seen in the figure, at a low ITON concentration (3 mg ml^{-1}), the RMS roughness was around 16.6 nm, and as the ITON concentration increased to 15 mg ml^{-1}, the surface roughness reached 46.8 nm. The increase in roughness can be attributed to the increasing ITON concentration, as the rough structure produced by ITONs helps trap air in the surface's gaps. This, coupled with the low surface energy of AF-2400, gave the nanocomposite films superhydrophobicity. However, increasing the ITON concentration over 15 mg ml^{-1} resulted in a negligible change in surface roughness, possibly due to the agglomeration of a higher concentration of ITONs forming a more continuous structure in the AF-2400 matrix. This behavior is consistent with that of the films' contact angles, which stayed almost constant because there was no notable change in surface roughness, even with increasing nanoparticle concentration. The trends in roughness development can be seen clearly in figure 2.

Figure 6(a) shows the surface morphology of composite films with various loading fractions of ITONs. Throughout this paper, we present the concentration of ITONs based on their initial loading fraction in the AF solution. Although it may be preferable to present the loading fraction in the ITON/AF composite, measuring the final concentration in a meaningful way is very challenging. We hypothesized, at least qualitatively, that the final concentration of ITONs in the composite films is directly proportional to the initial loading fraction of ITONs in AF solution. As seen in the images, the ITON particle concentration increases when the initial ITON loading fraction increases. This confirms our hypothesis, as well as the validity of presenting our results as a function of initial ITON loading fraction rather than the final concentration of ITONs in the composite films.

Figure 6(b) shows the EDS elemental mapping of In, Sn, C, and F in AF-2400/ITON nanocomposite films with an ITON concentration of 20 mg ml^{-1}, overlapped with SEM images of surface morphology. As seen from the elemental mapping, the concentration of In and Sn is highest at protuberances. This indicates that the protuberances are aggregated ITONs that are providing the sample's roughness. Similarly, C and F mapping showed thin coverage on ITON protuberances. The presence of F reduces surface energy and, hence, promotes superhydrophobicity.

3.3. Chemical surface analysis

XPS analysis was conducted on the nanocomposite films to show the effect of surface chemical composition on contact

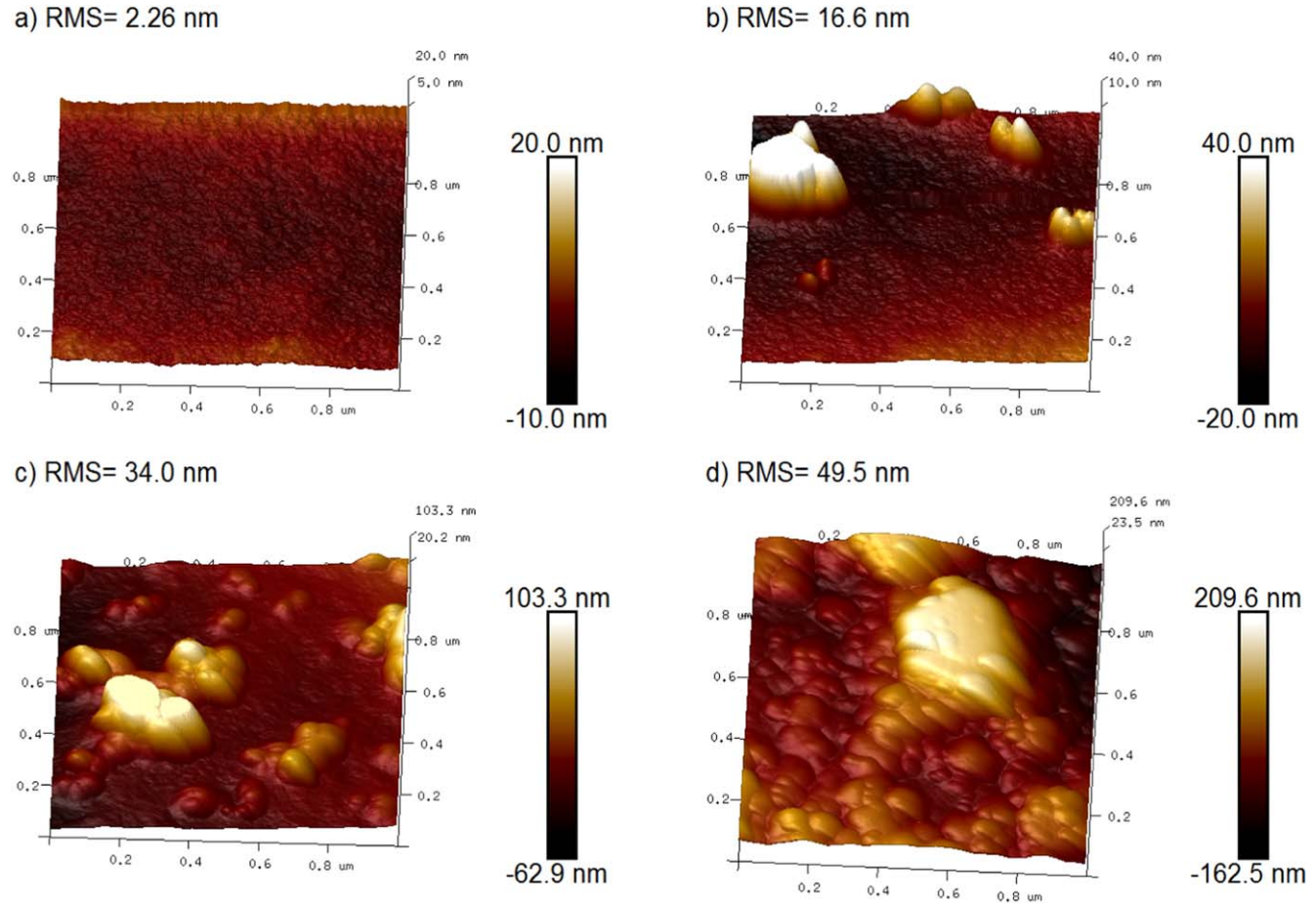

Figure 5. 3D AFM images (scan size 1 μm × 1 μm) for (a) pure AF-2400 and (b), (c), and (d) AF/ITON films with ITON concentrations of 3 mg ml^{-1}, 10 mg ml^{-1}, and 20 mg ml^{-1}, respectively.

angle. The XPS spectrum wide-scans of pure AF-2400 and AF-2400/ITON films with various concentrations are displayed in figure 7. As expected, the pure AF-2400 film had three major binding energy peaks: the peak at 292.4 eV is assigned to carbon bonded with fluorine (–CF2–) [22], the peak at 536.2 eV is attributed to oxygen in the dioxole ring, and the peak at 689.7 eV is attributed to the fluorine (Fs1) signal. These binding energy values agree with published data on the AF-2400 polymer [23].

Mixing low concentrations of ITONs (around 5 mg ml^{-1}) with AF-2400 did not change the chemical composition of the film surface, with all peaks appearing at the same binding energies as pure AF-2400. The only difference was a curve showing a small (negligible) amount of indium and tin elements, with binding energy located at 445.72 eV and 487.76 eV, respectively. These small percentages of In and Sn prove that the AF-2400 completely encapsulates the ITO nanoparticles. In fact, the ITO nanoparticles have an average size of less than 50 nm, much smaller than the ∼105 nm thick AF-2400. As the ITON concentration increased, the peaks of In and Sn became clearer (figure 7). It can be concluded, then, that increasing the ITON concentration to 15 mg ml^{-1} encourages aggregation of ITONs and, consequently, produces bigger particles. These particles were covered with a very thin layer of AF-2400, and the XPS could detect some of them, as the detection depth of XPS is 5–10 nm. At this concentration, the oxygen concentration increased by about 1%; this small addition in oxygen comes from the ITO nanoparticles. It seems that increasing the concentration of ITONs to 20 mg ml^{-1} caused some aggregated particles to grow, and these particles either were not covered by AF-2400 or were covered with a very thin layer; this caused the increase in In and Sn concentrations. Table 1 shows the elemental atomic composition of pure AF-2400 and AF-2400/ITON films.

3.4. Optical analysis

As a per-fluorinated amorphous polymer, Teflon AF-2400 has unique, extraordinary optical properties; ITON also has high transparency, around 90% [24]. Figure 8 gives the transmission spectrum for pure AF-2400 and the AF-2400/ITON composite film-coated glass substrates in the range of 300–1000 nm. The figure clearly shows that pure AF-2400 thin films have very high transparency, more than 98% in the near-infrared to ultraviolet range. At low ITON concentrations (less than 10 mg ml^{-1}), the AF-2400/ITON thin films also had very high transparency, around 95%—close to the

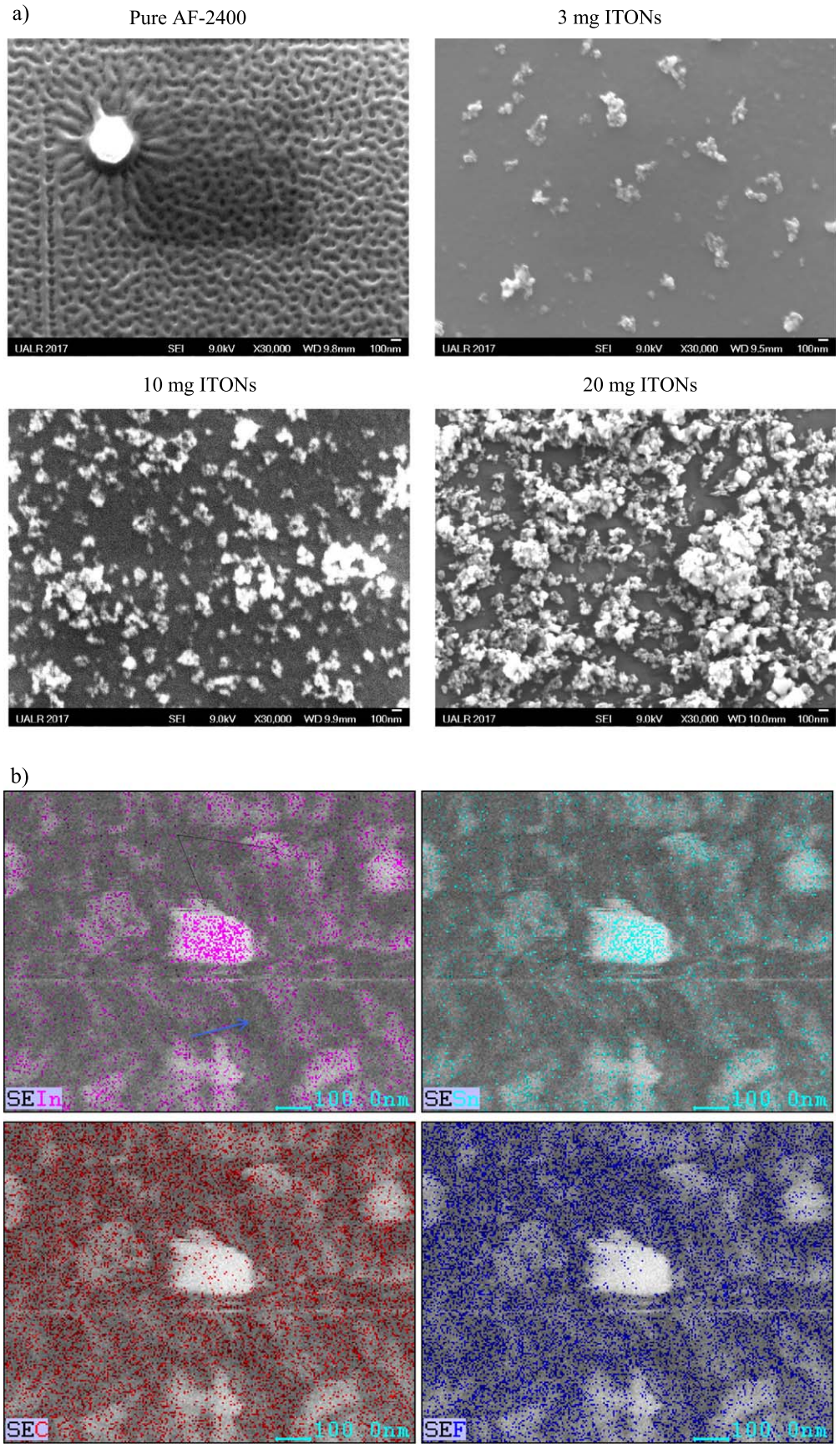

Figure 6. (a) SEM images of AF-2400/ITON nanocomposites with different ITON concentrations. (b) Elemental mappings of indium (In), tin (Tn), carbon (C), and fluorine (F) contained in the AF-2400/ITON nanocomposite film with 20 mg ml^{-1} of ITONs (100 000× magnification). Blue arrow: AF-2400, black arrows: ITON clusters.

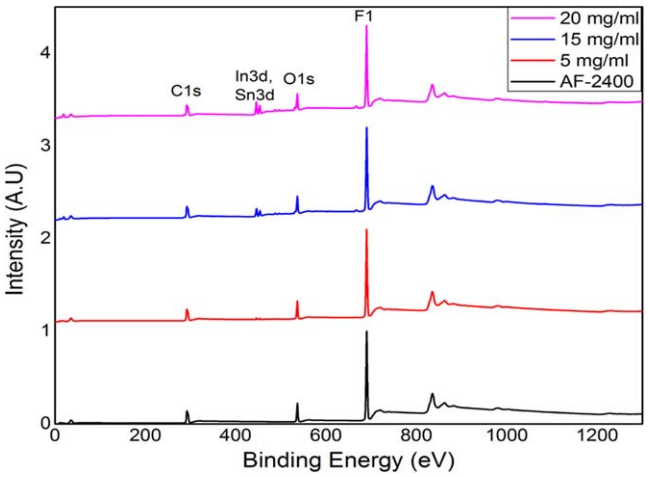

Figure 7. XPS spectrum of pure AF-2400 and AF-2400/ITON films with different ITON concentrations.

Table 1. Surface chemical composition of pure AF-2400 and AF-2400/ITON composites with various ITON concentrations.

Samples	C%	O%	F%	In	Sn
AF-2400	31.93	12.33	55.74	—	—
5 mg ml^{-1}	31.96	12.49	55.38	0.13	0.03
15 mg ml^{-1}	31.92	13.52	53.71	0.74	0.11
20 mg ml^{-1}	31.31	13.99	53.38	1.17	0.15

value of the pure AF-2400 film. So, because both the AF-2400 matrix polymer and ITON have very high transparency in the visible range, the AF-2400/ITON composite has high transparency at a low ITON concentration. Increasing the ITON concentration to 10–20 mg ml^{-1} did not significantly affect the optical properties, with transparency staying around 95% in the visible and IR range. However, at the 300 nm wavelength, the transparency of the AF-400/ITON thin films dropped between 73% and 61%. Increasing the ITONs to 30 mg ml^{-1} decreased the transmission considerably, to 73% in the visible range and 40% at 300 nm, due to the ITO nanoparticles aggregating, forming large particles, and blocking the light, which prevented it from passing through the film.

Figure 9 presents the effect that annealing temperature had on the transparency of the AF-2400/ITON composite films in the wavelength range 300–1000 nm. The figure shows that increasing the annealing temperature to 100 °C–330 °C has no significant effect on the transparency of the composite film. Figure 10 shows 20-μl colored water droplets on a bare glass substrate, AF-2400 polymer, and AF-2400/ITON composite film-coated glass substrate. The figure demonstrates the superhydrophobicity and high optical transmission of the AF-2400/ITON-coated substrates compared with a bare glass substrate. These qualities make the composite film a very promising coating for several practical applications.

3.5. Mathematical modeling of wetting behavior

The Wenzel model was the first theoretical model to describe the contact angle of a liquid on a rough surface (equation (1)). In this model, Young's equation, which describes a smooth surface, has been modified to describe surface wettability when drops of liquid penetrate the roughness grooves [25, 26]. The Wenzel equation determines the wettability of a surface—a surface with a contact angle $<90°$ is more hydrophilic, and a surface with a contact angle $>90°$ is more hydrophobic [27, 28].

$$\cos\theta_a = r\cos\theta, \tag{1}$$

where θ *and* θ_a are the equilibrium and apparent contact angles, respectively; r is the surface roughness ratio ($r = a/A$), a is the actual surface area, and A is the apparent area. The surface roughness factor (r) can be calculated from the equation below:

$$r = 1 + S_{dr}/100, \tag{2}$$

where S_{dr} (Developed Surface Area ratio) is the ratio between interfacial and projected area, providing for the additional surface area created by the roughness. Typically, S_{dr} is zero for a flat surface and increases with increasing surface roughness. Values of S_{dr} depend on a combination of the height of peak of the roughness peaks and the density of rough structures in the scanned region. S_{dr} parameter was determined from AFM imaging, with a scanning size of 1 μm × 1 μm.

However, if the drops of liquid do not penetrate the concavities of the surface, the Wenzel model will not apply. In this case, the Cassie–Baxter model can be used to predict the surface wettability of heterogeneous surfaces (composite of two different materials) [29]. The Cassie–Baxter model is more accurate for real surfaces than Wenzel's model. Equation (3) gives the Cassie–Baxter model for a mixed surface consisting of solid materials and air pockets [30].

$$\cos\theta_a = f_s r(\cos\theta + 1) - 1, \tag{3}$$

where *fs* is the solid fraction where the droplet sits partially on solid and partially on air pocket. Calculating the solid fraction (fs) of a randomly rough surface is the biggest challenge facing the Cassie–Baxter model.

Another formula for predicting the wettability of a randomly rough surface was produced by Shuttleworth and Bailey [31]. Their model proposes a relationship between the apparent and intrinsic angles of a rough surface. The equation is the sum of the intrinsic angle and maximum slope angle (α) of the surface at the drop contact point.

$$\theta_a = \theta + \alpha. \tag{4}$$

The maximum slope angle value will be positive for an advancing angle and negative for a receding angle. So, the apparent contact angle is less or greater than the inherent angle, depending on whether the latter is acute or obtuse more details can be found in references [25, 31, 32].

We applied the Wenzel, Cassie–Baxter, and Shuttleworth–Bailey models to compare the measured SCAs with theoretical data and to see the effect of ITON concentration

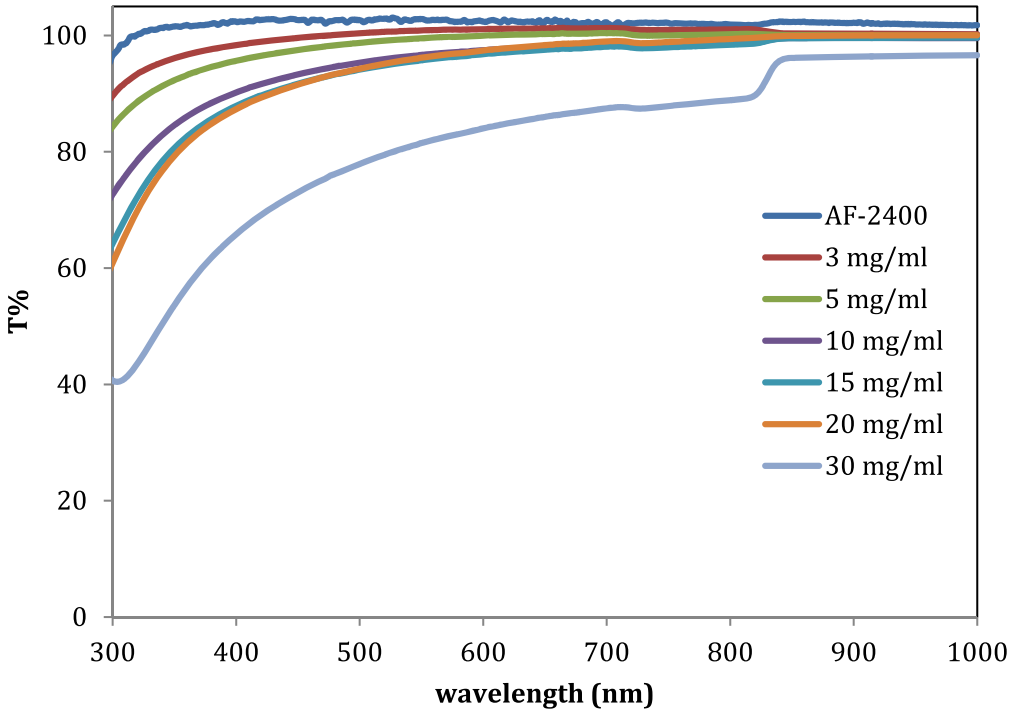

Figure 8. Transparency of AF-2400 and AF-2400/ITON composite thin films with different ITON concentrations on glass substrates.

on the water repellency of the AF-2400/ITON composite. Figure 11 compares the experimental and theoretical contact angles in relation to ITON concentration. It is clear that with increasing ITON concentration, the roughness factor (r) increases linearly due to the increasing surface roughness.

According to the Wenzel model, increasing the roughness factor (r) promotes the inherent wettability of a surface by increasing its surface area. In our experiments, the contact angles of the AF-2400/ITON composites increased linearly as the ITON concentration increased, aligning with the trend predicted by the Wenzel model, though the predicted contact angles were far from the real measured values of the superhydrophobic surfaces. According to the Wenzel model, to reach superhydrophobicity with a contact angle of $\sim$150°, the material's roughness factor should be $r \sim 2$, which required an increase in surface area in the range of 67%. However, in our experiments, the maximum roughness factor for the AF-2400/ITO thin film at the high ITON concentration was $r \sim 1.25$, and the film showed superhydrophobicity with a contact angle around 151°. These results confirm that the Wenzel model would be imperfect to illustrate the wettability of hydrophobic nanoparticle composites.

The Cassie–Baxter model involves another factor in its prediction of the wettability of any surface—the solid fraction (fs) (equation (3)). The major challenge of this equation is how to calculate the solid fraction for randomly rough surfaces. We calculated this by using ImageJ software to convert the original images of the prepared films to binary (8 bit) and then subtract the background. For this process, it was crucial to use a band pass filter to achieve good contrast. Finally, the '-Adjust-Threshold' step must be used to calculate the solid fraction percentage. This procedure was applied for all images in the same way. An example of a binary image converted by the ImageJ software, as well as the original SEM image, is shown in figure 12.

The experimental contact angles and the ones estimated by the Cassie–Baxter model are shown in figure 10 as a function of ITON concentration. At low ITON concentrations —less than 15 mg ml^{-1}—the contact angles were predicted to increase sharply to a very high value, more than 150°. This unrealistic prediction was based on an inaccurate solid fraction calculation because at low concentrations, the ITO nanoparticles are far away from each other. So, during the imaging process to obtain the solid fraction, the software calculates just the area of the ITONs, which is too small. Consequentially, the solid fraction is calculated as smaller than it is, leading to incorrect predicted contact angles. On the other hand, when the ITON concentration was increased to 15 mg ml^{-}1 and above, the experimental and predicted data matched adequately. In this stage, when the ITO nanoparticles start attaching to each other and producing small pores, it becomes more accurate to measure the solid fraction by the software. The pores help trap air and form air pockets; these pockets cover almost the entire sample area, making the solid fraction measurements easy and accurate to find. Therefore, it seems that the Cassie–Baxter model can be applied when high concentrations of ITONs are present and the surface becomes superhydrophobic, but not with low concentrations, when the surface is just hydrophobic.

As mentioned above, for randomly rough surfaces, predictions based on roughness factor alone are not accurate, and it is difficult to determine their solid fraction. To overcome these limitations of the Wenzel and Cassie–Baxter methods, we tried the Shuttleworth–Bailey model. The Shuttleworth–Bailey

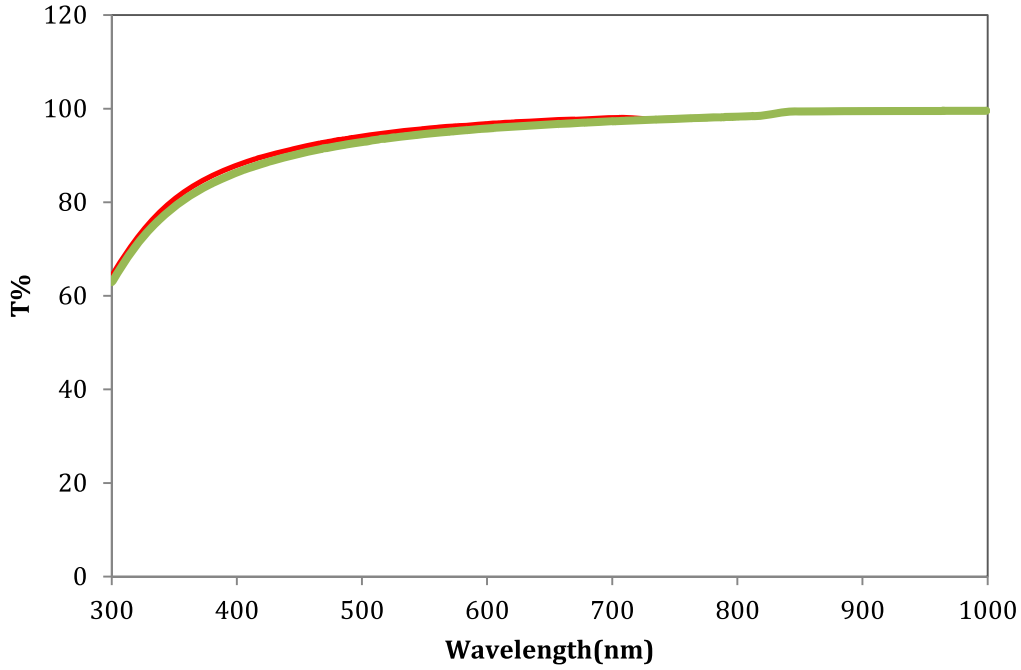

Figure 9. Effect of annealing temperature on the transparency of the AF-2400/ITON nanocomposite with 15 mg ml^{-1} concentration: 100 °C (red), 190 °C (blue) (red and blue lines overlap), and 330 °C (green).

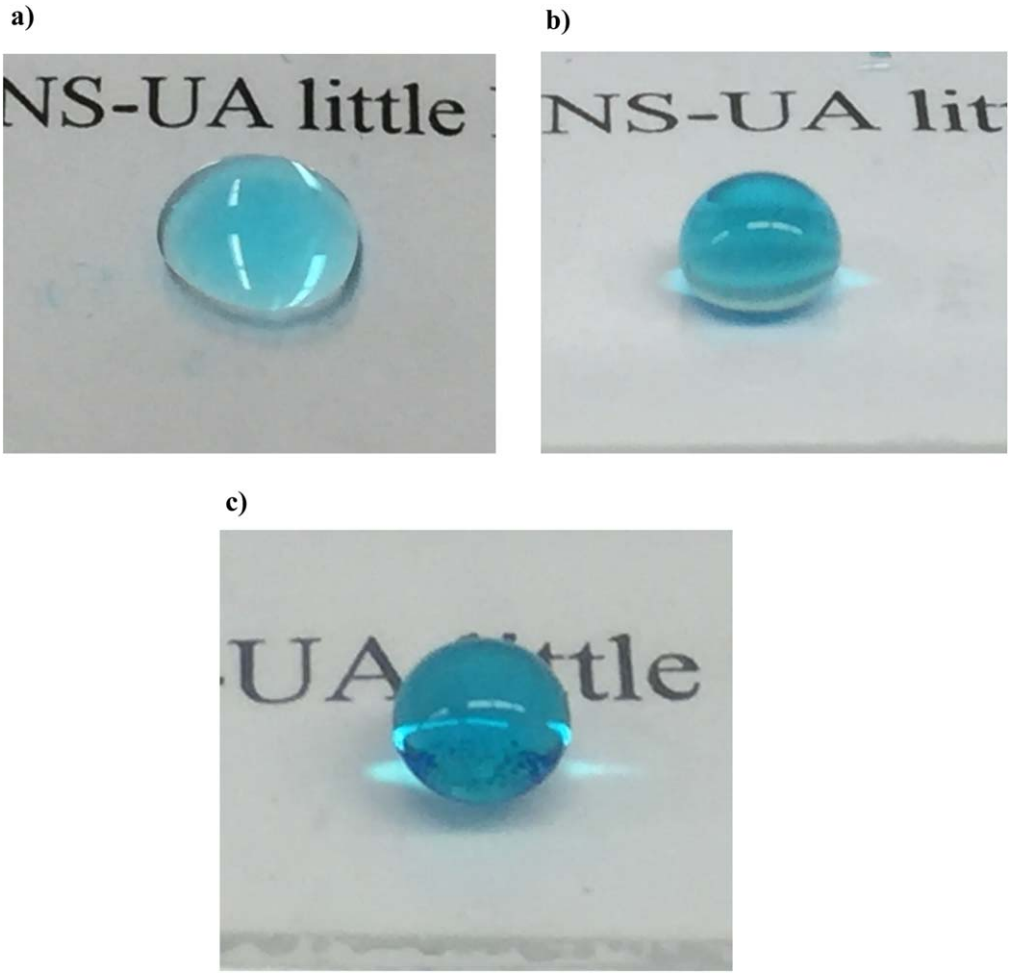

Figure 10. Photos of a 20 μl droplet on (a) bare glass, (b) pure AF-2400/glass, and (c) glass coated with 15 mg ml^{-1} of the AF-2400/ITON nanocomposite.

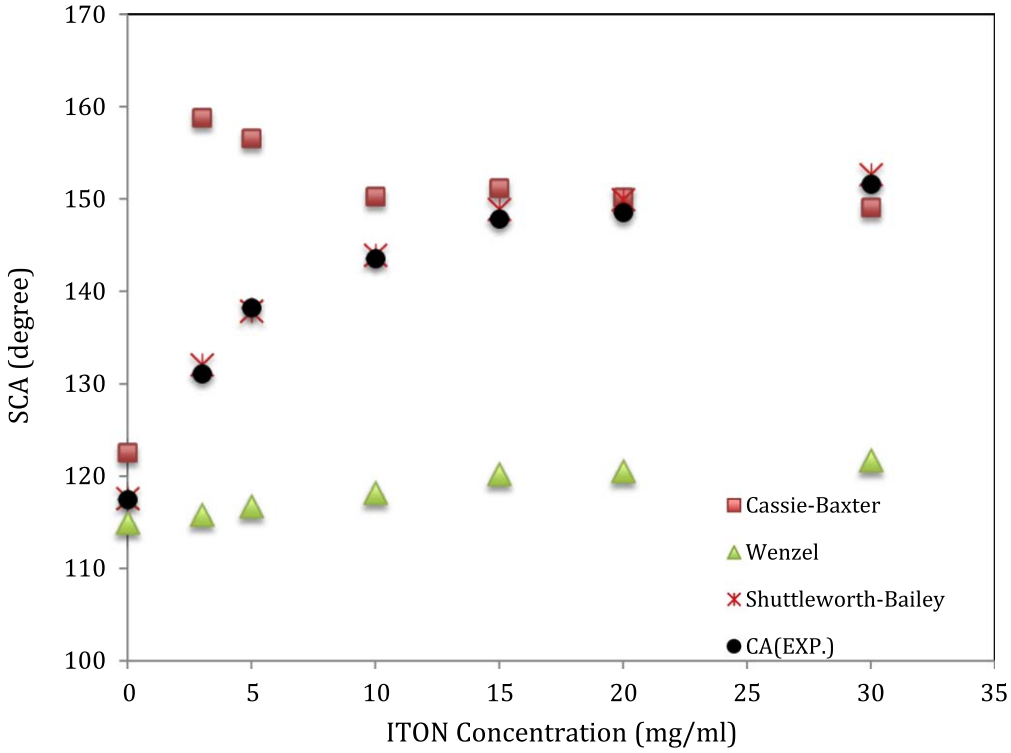

Figure 11. Comparison between experimental data and predictions by Wenzel, Cassie–Baxter, and Shuttleworth–Bailey models for the static contact angle of AF-2400/ITON nanocomposite as a function of ITON concentration.

equation depends totally on α parameter, as shown in equation (4). The α values for the composite films were obtained from AFM images of four different locations on each film, with the average being taken to estimate real value. The AFM height profile and the α values are shown in figure 13 for AF-2400/ITON composites with various ITON concentrations. The figure shows that the α values increase linearly with increasing ITON concentration. This result confirms that the α parameter is proportional to the surface roughness of the composite. Substituting α values in equation (4) for the equilibrium angle of pure AF-2400 (115°), the calculated contact angles are presented in figure 12. It is clear from the figure that the experimental and predicted contact angles follow the same trend and match well in all ITON concentrations (both low and high). So, we can conclude that the Shuttleworth–Bailey model accurately predicts the effect of the surface roughness of the AF-2400/ITON composites on their advancing contact angle. This model could be used to explain the wettability (advancing contact angle) of hydrophobic materials mixed with nanoparticles to increase surface roughness. However, the model is not as accurate for predicting the receding angle [25].

3.6. Optical transmittance simulation

Effective medium theories for an inhomogeneous medium consisting of pure particles (fillers) and homogenous medium (matrix) are used to study the dielectric properties of heterogeneous composites. The Maxwell-Garnett (MG) and Bruggemann models, known as effective medium approximation (EMA), are two such mathematical models. These models utilize the volume fraction of the fillers to explain the topology of materials. The MG model works well when the particle concentration is very low, there is a long distance between particles, and the particles have spherical or elliptical shapes [33]. When the particles are partially interconnected and have a percolation threshold fc $\geqslant$0.33, the Bruggemann model gives better approximation data. Looyenga introduced another simple effective medium model that depends on volume fraction as the tunable geometry parameter. In his model, the percolation strength also depends on the volume fraction [34]. Unfortunately, using volume fraction as the only fitting parameter to describe the topology of a complex composite makes the above models unsuitable in many cases, resulting in poor agreement between experimental and simulated data.

The general expression introduced by Bergman to describe the effective dielectric medium for complex phase-systems is called the Bergman representation. In addition to the normal fitting parameter, volume fraction, Bergman included a new function, spectral density (g), which is a normalized distribution function of geometrical resonances. These resonances depict the electric interaction between various parts of the system and are characteristic of the surface's micro-topology. The Bergman representation to calculate effective dielectric function ε_{eff} is given in equation (30); more details on this equation can be found in the references [35, 36].

$$\varepsilon_{eff} = \varepsilon_M \left(1 - (1 - v) \int_0^1 \frac{g(n, v)}{\frac{\varepsilon_M}{\varepsilon_M - \varepsilon} - n} dn \right), \qquad (5)$$

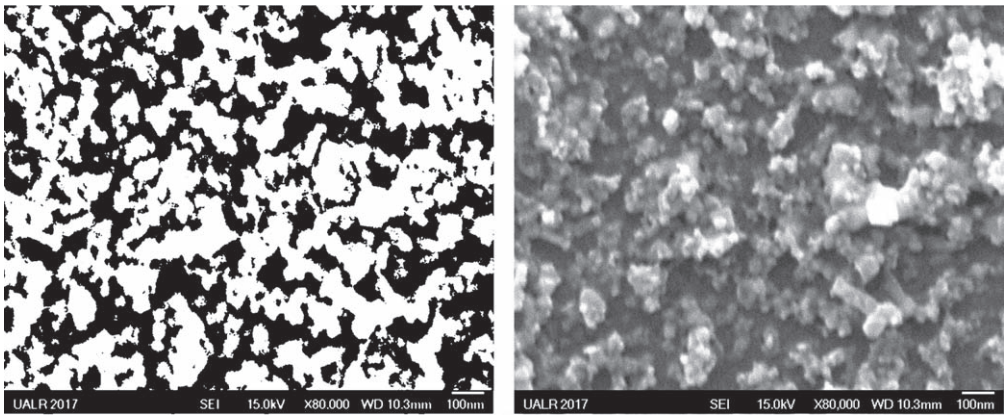

Figure 12. Images of a 20 mg ml^{-1}-concentration AF-2400/ITON thin film. Left: binary image treated with software to estimate solid fraction. Right: the original SEM image. The white area represents solid fraction and the black area is the porosity or air pockets.

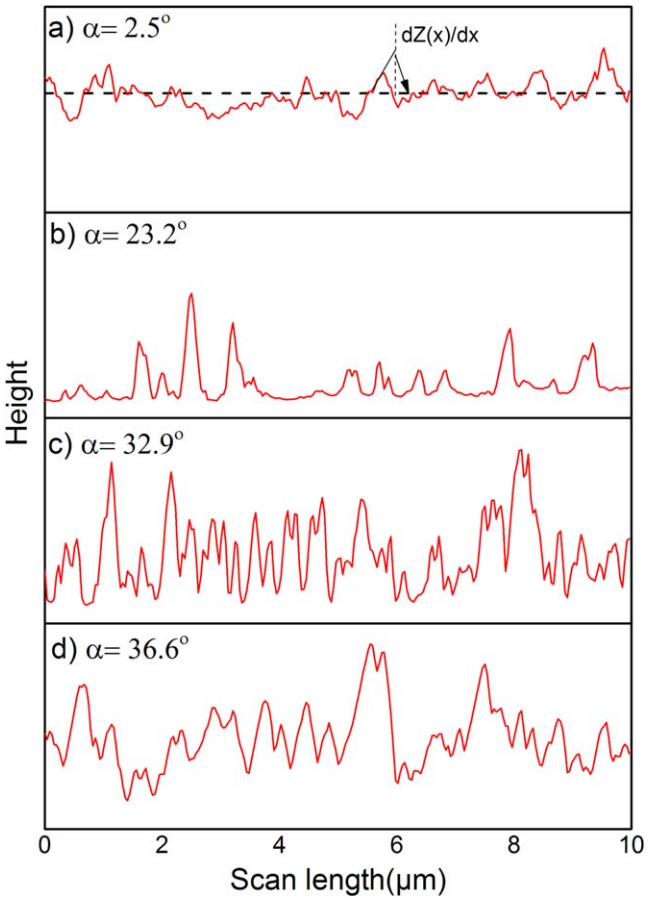

Figure 13. AFM height profiles of AF-2400/ITON nanocomposites were obtained under 1.0 Hz scan rate: (a) pure AF-2400, (b) 5 mg ml^{-1}, (c) 15 mg ml^{-1}, and (d) 30 mg ml^{-1}.

where ε_M, w_M, and ρ_M represent the dielectric constants, weight, and density of the matrix, (host) respectively.

$$\int_0^1 g(n, v)dn = 1$$
$$v = [\rho_M \cdot w_f/(\rho_M \cdot w_f + \rho_f \cdot w_M)], \quad (6)$$

where ε, v, w_f, and ρ_f represent dielectric constant, volume fraction, weight, and density of particles (fillers), respectively. The spectral density function g(n, v) depends only on the geometry of the heterogeneous mixture phase and is independent from the individual materials' properties. It is a real function and normalized in the interval [0, 1]. The Bergman representation is considered the more flexible parameterization model because it uses three main fitting parameters: volume fraction (v), percolation strength (Pc), and spectral density (g). That makes this model valid in all EMA systems [36].

In this work, the prepared heterogeneous system of AF-2400/ITON consists of ITONs as fillers and AF-2400 polymer as the matrix. A comparison between experimental and simulated data for the AF-2400/ITON composites is shown in figure 14. The simulation was done using SCOUT software from W. Thiess. Before the simulation process, the dielectric functions of the pure AF-2400 polymer and the ITONs were added to the database of the software [37] in order to calculate the optical transmittance of the AF-2400/ITON composite.

The approximate volume fraction for ITONs was estimated using equation (6), utilizing the weight and density of the AF-2400 polymer and ITON particles [38]. The thickness of the AF-2400/ITON composite can also be used as a fitting parameter, and we have a clear idea of composite thickness based on earlier data. At low ITON concentrations (5 mg ml^{-1}), the percolation strength can be set to zero because the ITON particles are far away from each other. In other words, there are no interconnected particles inside the composite. The known values—thickness, volume fraction, and percolation strength—were used as initial values to achieve the first fitting process. After that, the spectral density was set as the free fitting parameter until optimal fitting could be obtained; more details about the fitting process for spectral density can be found in W. Theiss software [37]. The ITON particles began to partially interconnect with each other and build a network of islands as the particle concentration increased, with a volume fraction of $v \geqslant 0.33$.

In the next phase of this research, we will work with percolation strength (Pc) values over zero for the 15 and 30 mg ml^{-1} concentrations to get optimal fitting. The agreement between experimental and simulated data is good in the visible range for both low- and high-volume fractions of

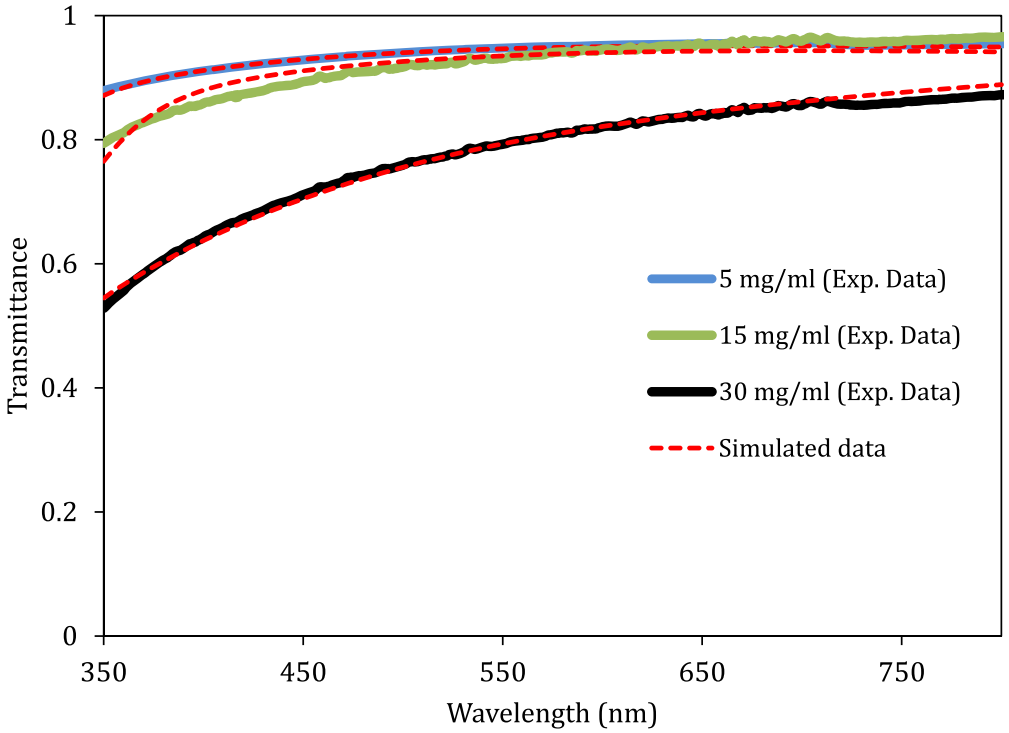

Figure 14. Optical transmittance of AF-2400/ITON nanocomposites. Experimental data: solid lines; simulated data: red dashed lines.

Table 2 Comparison between experimental and simulated data for AF-2400/ITON composites.

Samples (ITON Cons.)	Thickness (nm) (Exp. ±9)	Thickness (nm) (simulated)	Volume fraction (equation (2))	Volume fraction (simulated)	Percolation strength (simulated)
5 mg ml^{-1}	100.2	116	0.33	0.23	0
15 mg ml^{-1}	101	120	0.57	0.56	0.62
30 mg ml^{-1}	109	105	0.76	0.72	0.97

ITON. Table 2 shows the measured and simulated data calculated by SCOUT software. The film thickness and volume fraction seem to be close, supporting our simulation process. Finally, the Bergman representation was used because it gave us better results than the other classical models, which had poor agreement spatially in the high volume fractions.

4. Conclusion

Superhydrophobic and highly transparent Teflon® AF-2400/ITON coatings were prepared successfully using spin coating. AF-2400/ITON nanocomposites with different ITON concentrations were deposited on glass substrates. The low surface energy of the AF-2400 polymer and the roughness provided by the ITONs helped give the surfaces water roll-off properties, with SCAs around 152° and CAH less than 2°. The Wenzel and Cassie–Baxter methods produced expected results but had some limitations, while the Shuttleworth–Bailey model matched with our measured data for the AF-2400/ITON nanocomposite excellently. The extraordinary optical properties of AF-2400 and ITONs provided the films with excellent transparency—around 95% in the visible and near-IR range. The Bergman representation, an effective medium theory, provided good agreement between the films' measured and simulated transmittance in the visible range. Studying the effect of spin coating speed showed that a spin speed less than 3000 rpm is optimal to create a good superhydrophobic coating. In addition, annealing temperatures less than 250 °C are favorable for producing superhydrophobic coatings with high SCAs and transparency. The addition of ITO nanoparticles helped increase the roughness of the nanocomposite films but did not appear to affect overall thermal stability of AF-2400. The XPS results showed that, while the chemical surface properties of AF-2400 give it low surface energy, the nanoparticles created nano- or microstructures in the AF-2400 matrix, making it rough and, as a result, promoting superhydrophobicity. Because of these properties, AF-2400/ITON coatings have many potential uses, including industrial applications, solar cell coatings, and liquid waveguides.

Acknowledgments

Funding for this research was provided by the Center for Advanced Surface Engineering under National Science

Foundation grant no. IIA-1457888 and by the Arkansas EPSCoR Program, ASSET III. The editorial assistance of Emily Davis is also acknowledged.

ORCID iDs

Ganesh K Kannarpady https://orcid.org/0000-0003-1666-8139

References

[1] Xu L, Karunakaran R G, Guo J and Yang S 2012 Transparent, superhydrophobic surfaces from one-step spin coating of hydrophobic nanoparticles *ACS Appl. Mater. Interfaces* **4** 1118–25
[2] Ebert D and Bhushan B 2012 Transparent, superhydrophobic, and wear-resistant coatings on glass and polymer substrates using SiO_2, ZnO, and ITO nanoparticles *Langmuir* **28** 11391–9
[3] Basu B J and Dinesh Kumar V 2011 Fabrication of superhydrophobic nanocomposite coatings using polytetrafluoroethylene and silica nanoparticles *ISRN Nanotechnology* **2011** 803910
[4] Michael A N, Robert J D and Jonathan P R 2010 A novel and inexpensive technique for creating superhydrophobic surfaces using Teflon and sandpaper *J. Phys. D: Appl. Phys.* **43** 045301–5
[5] Wang K, Xiong P, Xu X, Wang K, Li Y and Zheng Y 2017 Chemically robust carbon nanotube—PTFE superhydrophobic thin films with enhanced ability of wear resistance *Prog. Nat. Sci.: Mater. Int.* **27** 396–9
[6] Zhuang A, Liao R, Dixon S C, Lu Y, Sathasivam S, Parkin I P and Carmalt C J 2017 Transparent superhydrophobic PTFE films via one-step aerosol assisted chemical vapor deposition *RSC Adv.* **7** 29275–83
[7] Alawajji R A, Kannarpady G K and Biris A S 2018 Fabrication of transparent superhydrophobic polytetrafluoroethylene coating *Appl. Surf. Sci.* **444** 208–15
[8] Scheirs J 1997 *Modern Fluoropolymers: High Performance Polymers for Diverse Applications* (New York: Wiley)
[9] Kim H-M, Sohn S and Ahn J S 2013 Transparent and super-hydrophobic properties of PTFE films coated on glass substrate using RF-magnetron sputtering and Cat-CVD methods *Surf. Coat. Technol.* **228** Supplement 1 S389–92
[10] Yasuyuki T, Hisanori A, Etsuo Y and Akira I 2002 Pulsed laser deposition of poly(tetrafluoroethylene), poly (methylmethacrylate), and polycarbonate utilizing anthracene-photosensitized ablation *Japan. J. Appl. Phys.* **41** 885
[11] Yasuoka H, Yoshida M, Sugita K, Ohdaira K, Murata H and Matsumura H 2008 Fabrication of PTFE thin films by dual catalytic chemical vapor deposition method *Thin Solid Films* **516** 687–90
[12] Bazin N, Andrew E and Mclnes H A 1999 Formation of Teflon AF polymer thin films as optical coatings in the high-peak-power laser field *Proc. SPIE* **3492** 964–9
[13] Yang M K and French R H 2008 Optical Properties of Teflon® AF Amorphous Fluoropolymers *Proc. SPIE* **7** 033010–1
[14] Thomas I M and Campbell J H 1991 Novel Perfluorinated Antireflective and Protective Coating for KDP and other Optical Materials *Proc. SPIE* **1441** 294–303
[15] Altkorn R, Koev I and Pelletier M J 1999 Raman performance characteristics of Teflon®-AF 2400 liquid-core optical-fiber sample cells *Appl. Spectrosc.* **53** 1169–76
[16] Dress P and Franke H 1996 A cylindrical liquid-core waveguide *Appl. Phys.* B **63** 12–9
[17] Takiguchi H, Tsubata A, Miyata M, Odake T, Hotta H, Umemura T and Tsunoda K-I 2006 Liquid Core waveguide spectrophotometry for the sensitive determination of nitrite in river water samples *Anal. Sci.* **22** 1017–9
[18] Drummond C J, Georgaklis G and Chan D Y C 1996 Fluorocarbons: surface free energies and van der Waals interaction *Langmuir* **12** 2617–21
[19] Tavana H, Petong N, Hennig A, Grundke K and Neumann A W 2005 Contact angles and coating film thickness *J. Adhes.* **81** 29–39
[20] Scarratt L R J, Hoatson B S, Wood E S, Hawkett B S and Neto C 2016 Durable superhydrophobic surfaces via spontaneous wrinkling of Teflon AF *ACS Appl. Mater. Interfaces* **8** 6743–50
[21] Shim M H, Kim J and Park C H 2015 Development of superhydrophobic fabrics by surface fluorination and formation of CNT-induced roughness *Mater. Sci.* **21** 1392–20
[22] Fu R K Y, Mei Y F, Wan G J, Siu G G, Chu P K, Huang Y X, Tian X B, Yang S Q and Chen J Y 2004 Surface composition and surface energy of Teflon treated by metal plasma immersion ion implantation *Surf. Sci.* **573** 426–32
[23] Matienzo L J, Zimmerman J A and Egitto F D 1994 Surface modification of fluoropolymers with vacuum ultraviolet irradiation *J. Vac. Sci. Technol.* A **12** 2662–71
[24] Tao P, Viswanath A, Schadler L S, Benicewicz B C and Siegel R W 2011 Preparation and optical properties of indium tin oxide/epoxy nanocomposites with polyglycidyl methacrylate grafted nanoparticles *ACS Appl. Mater. Interfaces* **3** 3638–45
[25] Miller J D, Veeramasuneni S, Drelich J, Yalamanchili M R and Yamauchi G 1996 Effect of roughness as determined by atomic force microscopy on the wetting properties of PTFE thin films *Polym. Eng. Sci.* **36** 1849–55
[26] Wenzel R N 1936 Resistance of solid surfaces to wetting by water *Ind. Eng. Chem.* **28** 988–94
[27] Hazlett R D 1990 Fractal applications: wettability and contact angle *J. Colloid Interface Sci.* **137** 527–33
[28] Khedir K R, Kannarpady G K, Ishihara H, Woo J, Ryerson C and Biris A S 2011 Design and fabrication of teflon-coated tungsten nanorods for tunable hydrophobicity *Langmuir* **27** 4661–8
[29] Cassie A B D and Baxter S 1944 Wettability of porous surfaces *Trans. Faraday Soc.* **40** 546–51
[30] Cassie A B D 1948 Contact angles *Discuss. Faraday Soc.* **3** 11–6
[31] Shuttleworth R and Bailey G L J 1948 The spreading of a liquid over a rough solid *Discuss. Faraday Soc.* **3** 16–22
[32] Hitchcock S J, Carroll N T and Nicholas M G 1981 Some effects of substrate roughness on wettability *J. Mater. Sci.* **16** 714–32
[33] Maxwell Garnett J C 1904 XII. Colours in metal glasses and in metallic films *Phil. Trans. R. Soc.* A **203** 385
[34] Looyenga H 1965 Dielectric constants of heterogeneous mixtures *Physica* **31** 401–6
[35] Bergman D J 1978 The dielectric constant of a composite material—a problem in classical physics *Phys. Rep.* **43** 377–407
[36] Theiß W 1997 Optical properties of porous silicon *Surf. Sci. Rep.* **29** 91–192
[37] W Theiss 2017 Hard- and software for optical spectroscopy *Scout tutorial* http://wtheiss.com
[38] Messiry M E 2013 Theoretical analysis of natural fiber volume fraction of reinforced composites *Alexandria Eng. J.* **52** 301–6